SERBIAN JOURNAL OF ELECTRICAL ENGINEERING
Vol. 21, No. 2, June 2024, 163-185
UDC: 681.5:621.314.222 **DOI: https://doi.org/10.2298/SJEE2402163V**

A Search for Suitable Mother Wavelet in Discrete Wavelet Transform Based Analysis of Acoustic Emission Partial Discharge Signals

Shanmukha Reddy Vippala[1], Gururaj Sudhindra Punekar[1], Krishnan Chemmangat[1], Bhavanishanker Tangella[2]

Abstract: Signal processing helps monitor the condition of power equipment. Partial discharge (PD) signals used in condition-based maintenance give crucial information in the diagnosis of degradation of insulation. The acoustic emission technique (AET) is one of the most widely used techniques in PD signal analysis due to its inherent advantages. Analyzing acoustic emission partial discharge (AEPD) signals in the wavelet-domain provides critical insights into the location and type of the sources of PD. Selection of the most suitable mother wavelet in applying discrete wavelet transform (DWT) on AEPD signals is important as it will directly impact the outcome. For this selection, 36 wavelets belonging to the Daubechies, Symlets, Coiflets, and Bi-orthogonal families are investigated. For this purpose, five experimentally collected AEPD test signals are used. The selection is based on the "accuracy of wavelet decomposition results" in this work, probably for the first time. One mother wavelet from each family is individually shortlisted for all three performances, namely (a) reconstruction, (b) denoising, and (c) compression, by computing and comparing their commonly used metrics. Further, based on percentage energy criteria, the most suitable mother wavelets are identified as coif3, coif4, and coif5, respectively, for the three performances.

Keywords: Acoustic emission partial discharge (AEPD), Condition monitoring, Discrete wavelet transform (DWT), Mother wavelet, Multi-resolution analysis (MRA), Oil insulation, Power transformer.

1 Introduction

Power transformers are indispensable in supplying power to Agricultural, Commercial, Domestic, and Industrial loads. Therefore, condition-based maintenance (CBM) is necessary to avoid unexpected power transformer breakdowns, reducing associated revenue losses [1, 2]. Past experiences indicate that transformer

[1]Department of Electrical and Electronics Engineering, National Institute of Technology Karnataka, Surathkal, Mangalore 575025, India; E-mails: shanmukhareddyvippala.217ee012@nitk.edu.in; gsp@nitk.edu.in; cmckrishnan@nitk.edu.in
[2]Central Power Research Institute, Bangalore, Karnataka, India; E-mail: tbs@cpri.in

oil/paper insulation degradation is the primary cause of breakdown [3]. A problem with the insulation must be identified early in its nascent stages (incipient fault). Such problems can be identified by temperature measurements (hot-spot), gas-in-oil test by dissolved gas analysis (DGA), partial discharge (PD) measurements, and moisture analysis [1]. Among these, PD signals appear right at the initial stage of degradation of the insulation [4]. Due to this inherent advantage and its being a non-destructive technique (NDT), the PD detection method is suitable for monitoring the transformer insulation system. The PD in insulation systems manifests in heat, acoustic signals (sound), visible light signals, chemical changes, and electromagnetic waves (UHF signals) [4, 5 – 7]. Among these, the acoustic emission technique (AET) is one of the most suitable ways to measure PD indirectly due to its immunity to electromagnetic noise and interferences [5, 8]. The acoustic signals acquired by Piezoelectric sensors are in the time-domain. However, additional information can be retrieved by transforming it into the frequency-domain. The acoustic emission partial discharge (AEPD) signals are transient, irregular, and non-periodic [8]. In such cases, conventional Fourier transform loses time traces about the various frequencies emerging and extinguishing randomly [6, 9]. For such cases, time-frequency (T-F) analysis is more suited [10]. In T-F analysis, the wavelet transform adopts variable wavelet windows for analyzing long-duration-low-frequency components and short-duration-high-frequency components present in the signal [6, 9]. The wavelet transform of a time-domain signal generates a two-dimensional (2-D) array of wavelet coefficients [6, 11].

Researchers have applied the wavelet transform in the areas like hydraulic systems, to extract fault features, medicine for efficient diagnoses, and seismology for analysis. There have been quite a few attempts to use the wavelet transform in PD-based fault diagnosis and localization in electrical equipment [2, 7, 12]. In one such effort, the wavelet transform with ‘db2’ as the mother wavelet and a 6-level decomposition is used to extract the PD signals from a transformer [12]. The ‘bior2.6’ wavelet is used for DWT analysis of PD signals of an HVDC system in gas-insulated switchgear [7]. To distinguish between PD sources and their localization, DWT is applied with the ‘db4’ mother wavelet for the UHF-PD signals generated in power transformers [2]. The wavelet analysis of AEPD signals can be performed to (a) estimate the rate of deterioration of the insulation, (b) determine moisture levels, (c) detect particles, (d) locate the source of a PD, and (e) classify the type of PDs based on feature extraction [6, 8, 13 – 15]. In [6], CWT using the ‘Morlet’ wavelet and DWT using the ‘sym8’ wavelet up to a 7-level decomposition was applied to the acoustic emission pulses generated by types of PDs. The ‘db8’ mother wavelet with a 9-level decomposition is chosen for DWT of AEPD signals in identifying patterns of moisture contamination in transformer insulating oil [13]. The ‘db15’ mother wavelet and a 5-level decomposition are used to classify PDs occurring in oil-filled transformers

through measured AEPD signals [8]. The 'Haar' mother wavelet with 10 decomposition levels is applied to perform analysis using AET for PD localization in oil [14]. In [15], the 'Haar' wavelet up to 13 levels is utilized for particle identification through AEPD measurements in transformer oil.

Analyzing a signal with different wavelets gives results that are not unique [16]. Wavelet analysis decomposes the signal into several frequency levels (or sub-bands). The number of levels to which a signal is decomposed also plays a significant role in fetching beneficial information. Therefore, the present work attempts to select a suitable mother wavelet and its decomposition levels in the wavelet analysis of an AEPD signal.

The selection of the mother wavelet can be achieved using either a qualitative or a quantitative approach. The qualitative approach utilizes properties of the mother wavelet, such as its compact support, vanishing moments, regularity, singularity, symmetry, orthogonality, support width, the existence of scaling function, and the degree of shift variance. Generally, it is hard to arrive at a final decision on mother wavelet selection since more than one mother wavelet has similar properties. The quantitative approach utilizes statistical parameters like "maximum cross-correlation coefficient", "maximum normalized correlative energy", "mean description length (MDL)", and "variances of the CWT coefficients" in arriving at the suitable mother wavelet [16].

In most previous works, the mother wavelets are selected based on the similarities between the mother wavelet and the acquired signal. It has been observed that such a similarity is only sometimes adequate since the most similar wavelet (to the acquired signal) may not always be suitable for wavelet-based signal processing. On the contrary, mother wavelet selection based on the "accuracy of wavelet decomposition results" is highly recommended [16]. Hence, in the present work, the mother wavelet selection is attempted based on the "accuracy of wavelet decomposition results" using experimentally collected AEPD signals. In all, 36 mother wavelets are compared using three performances: reconstruction, denoising and compression to identify the suitable mother wavelet.

2 Fundamental Concepts

2.1 AEPD signal and measurement

Degradation and aging of insulation are significant causes of the failure of power apparati. These are caused by electrical, mechanical, environmental, and thermal stresses [5, 8, 17, 18]. Aging and degradation caused by these stresses result in a PD signal. The PD resulting in incipient faults can be detected by its manifestations like electromagnetic waves, sound, chemical changes, heat, light, and vibration. In the context of a power transformer, the AE signals caused by

PDs inside it travel in the form of waves and can be detected by an acoustic sensor placed on its body [13].

A PD is a localised electrical discharge in an insulation system that can lead to deterioration, aging, and failure of electrical power equipment like a transformer. Conducting on-site electrical PD tests necessitates extensive arrangements and temporary removal of the power transformer from service. Challenges arise in accurately measuring electric PD magnitudes due to electromagnetic interference and background noise. Consequently, alternative non-conventional on-line techniques have been developed to address these issues. Of these methods, AET is notably advantageous. PD activity in the insulation system leads to acoustic signal emission. Due to PD, sudden release of energy in a material generates elastic waves (acoustic waves) that travel through the material. These AEPD signals are detected by a sensor and are analysed for valuable insights. AEPD signal's capability to detect and localise discharge events in real time makes it a valuable tool for the monitoring and maintenance of transformers. AET is a non-destructive and non-invasive method, allowing its application to power transformers while they are in service, thereby eliminating the need for power interruption [5].

Piezoelectric sensors are the most commonly used acoustic emission sensors [1, 5]. Silicon grease is used as a couplant between the wall of the tank and the sensor [5, 8]. The acoustic waves are in the ultrasound frequency range, i.e. 20 kHz to 1 MHz [14]. Typical acoustic applications include acoustic ranging, seismology, acoustic localization, sonar, engine testing, vibration analysis, ocean acoustic tomography process control, and bioacoustics. This paper deals with AEPD signals and analysis.

2.2 Wavelet transform

The wavelet transform of a signal is obtained by computing the correlation coefficients between the signal and mother wavelet at desired scales s and time instants τ. Here the scale represents a band of frequencies [6, 8]. The wavelet transform of a signal is commonly implemented in two different ways: (a) continuous wavelet transform (CWT) and (b) discrete wavelet transform (DWT). The terms continuous and discrete do not refer to the nature of the signal: instead, they refer to the nature of the scale axis adopted [9]. CWT uses a continuous set of scales and causes redundancy by computing many more coefficients than necessary, consequently increasing the computational cost [7, 11]. Compact representations are desirable for energy calculations, signal compression, signal representation, and other types of analysis. Therefore, CWT, evaluated at specific scales is then called DWT, and this helps in minimizing the number of coefficients used [9]. DWT can be treated as the discretized version of CWT [10]. Nevertheless, CWT has gained importance for (a) the detection of oscillatory features, (b) singularity/regularity detection, (c) estimation of instantaneous

frequencies, and (d) filtering and feature extraction. The DWT of a signal $f(t)$ using mother wavelet ψ is defined using (1). Here m can be described as a discretized version of scale s denoted by $s = 2^m$ (dyadic scaling), and n is the discretized version of translation parameter τ denoted by $\tau = n2^m$ [6, 7]. In (1), symbol * denotes the complex conjugate of wavelet ψ. The wavelet at scale $s = 1$ or level $m = 0$ is called the mother wavelet. The wavelets with scales $0 < s < 1$ and $s > 1$ result in compression and dilation of mother wavelets, respectively, referred to as daughter wavelets [6].

$$\boldsymbol{T}(m,n) = \int_{-\infty}^{+\infty} f(t) \frac{1}{\sqrt{2^m}} \psi^* \left(\frac{t - 2^m n}{2^m} \right) \mathrm{d}t \,. \tag{1}$$

In DWT, mother wavelets do not have analytical expressions. Instead, each mother wavelet possesses corresponding decomposition high pass g_d[n] and low pass h_d[n] filters as well as reconstruction high pass g_r[n] and low pass h_r[n] filters with coefficients of certain length [6, 19]. The mother wavelet functions are evaluated from these filter coefficients iteratively [20]. Multi-resolution analysis (MRA) is a widely implemented decomposition tool in DWT to study different frequency sub-bands with appropriate time resolutions [6, 7]. In MRA, initially, the acquired discrete signal is treated as the best approximation coefficients available and is denoted as band A0, which has the frequency information of $[0 - f_{max}]$. The maximum detectable frequency (f_{max}) is half of the sampling frequency (f_s) given by Nyquist criteria. The decomposition of a signal at each stage is a two-step process. First, the available coefficients are convolved with the h_d[n] and g_d[n] filters for low-frequency and high-frequency components, respectively. Then, they are down-sampled by 2 to avoid overlapping frequency sub-bands [18, 21]. At the end of this 1st stage, the decomposition results in a set of approximation coefficients and detailed coefficients referred to as the A1 and D1 sub-bands with $[0 - f_{max}/2]$ and $[f_{max}/2 - f_{max}]$ frequencies, respectively [12, 22]. The approximation coefficients contain low-frequency components (also known as global features), and the detail coefficients contain high-frequency components (also known as local features) [14, 23]. In the next stage, sub-band A1 is further decomposed into low-frequency components sub-band A2 and high-frequency components sub-band D2. The detailed coefficients' sub-band D1 is left undisturbed. Generally, in MRA, an N-level decomposition of a signal results in N-detail levels {D1, D2, D3, …, DN} and one approximation level AN [6, 9, 23]. The inverse process is adopted to reconstruct the signal in the time-domain [18]. The approximation and detailed coefficients are up-sampled first and then convolved with reconstruction filters h_r[n] and g_r[n] [7, 9, 23]. The primary applications of DWT are (a) discontinuity detection, (b) signal compression, (c) denoising, and (d) signal estimation [9]. MATLAB toolboxes facilitate obtaining the wavelet transform and are used in the present study.

3 Methodology

3.1 Experimental set-up and data acquisition system

The AEPD time-domain signals used in this paper for analysis are generated in an experimental setup having a point-plane electrode system available in the central power research institute (CPRI), Bangalore, India. The experimental tank is made of mild steel and has the dimensions 1.1 m × 1.1 m × 1.1 m. EHV grade transformer oil is filled in the tank having wall thickness of 5 mm. The tip diameter of the point electrode is 30 μm, and a gap distance of 0.42 m is maintained between the point and bottom of the tank treated as the plane electrode [24, 25]. The AE workstation is a DSP based 16 channel data acquisition system. It consists of 4 channel DSP boards of 4 numbers for data acquisition from 16 piezoelectric AE sensors (model DT15i of M/s PAC, USA). Each AE sensor has a frequency range of 10 kHz – 1 MHz and a resonant frequency of 150 kHz, with an integrated preamplifier of 40dB gain. These 16 sensors are mounted on the outer wall of the experimental transformer tank using the acoustic couplant. The experimental setup of the transformer test tank having a point-plane electrode system is shown in Fig. 1. The current study uses a high voltage source of 0 – 75 kV (and 1.1 A) rating to generate PDs.

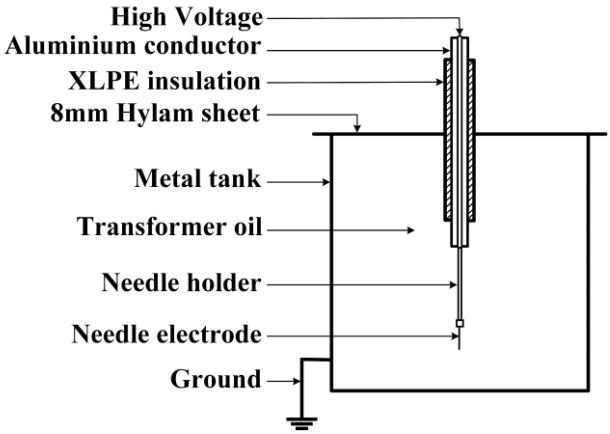

Fig. 1 – *Experimental setup of transformer oil tank with point-plane electrode system to generate PD.*

Figs. 2a – e illustrate the 5 AEPD signals employed in this analysis. These are the time domain signals obtained from the experimental set-up. These signals are obtained by randomly placing the sensors on the walls of the transformer model, which, in general, simulates an actual situation. Not too much can be inferred from these time domain signals. However, techniques like DWT analysis can give additional insights.

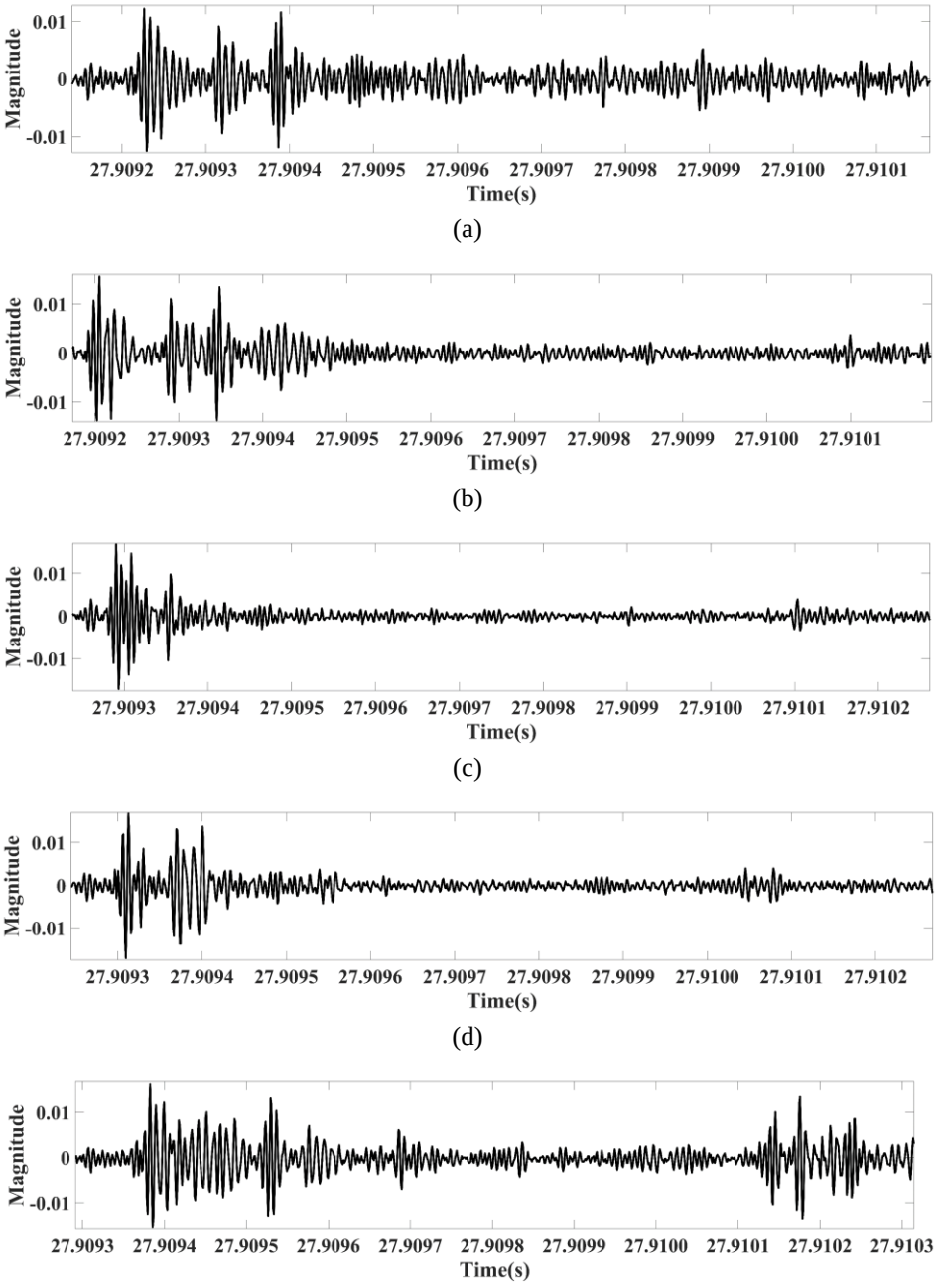

Fig. 2 – *Five typical acoustic emission partial discharge (AEPD) signals in time-domain used in the present analysis.*

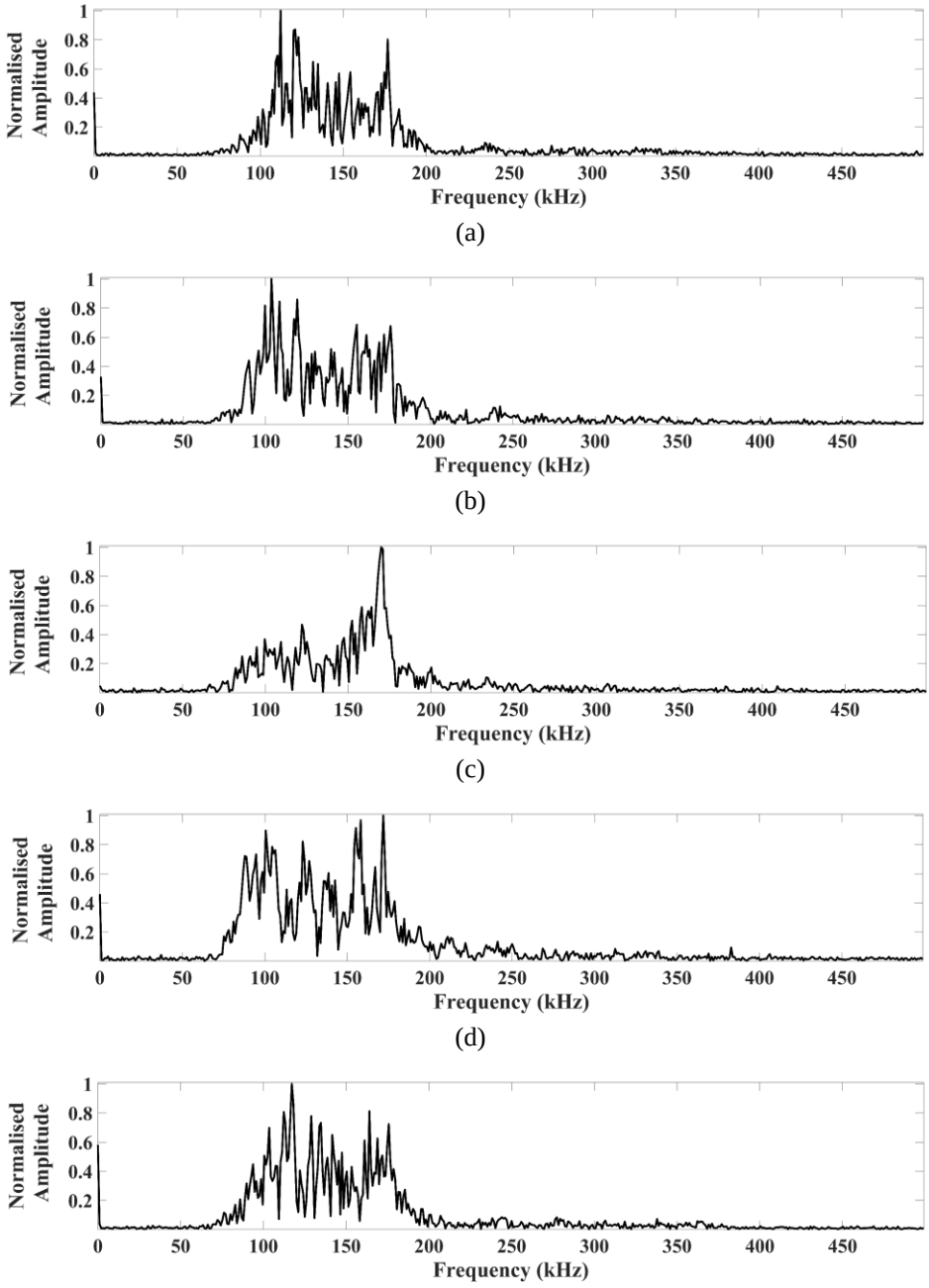

Fig. 3 – *Fourier spectrum of 5 acoustic emission partial discharge (AEPD) signals used in the present analysis.*

Figs. 3a – e present the Fourier spectrum of the 5 AEPD signals employed in this study. Spectral analysis reveals that the predominant energy is within the frequency range of 50 kHz to 250 kHz. Notably, this frequency range remains consistent across all 5 samples. Adhering to the Nyquist criteria, a minimum sampling frequency of 500 kHz is necessary for a maximum detectable frequency of 250 kHz. Hence, a sampling frequency of 1 MHz has been selected, and each signal length is of 1024 samples.

3.2 Analysis using DWT

The present work is limited to choosing a suitable mother wavelet for the DWT of AEPD signals. The mother wavelets of the Daubechies, Coiflets, Symlets, and Bi-orthogonal families were considered for analysis and are listed in **Table 1** [21]. These 36 mother wavelets are used in comparing their performance in AEPD analysis. A brief introduction to these wavelet families is given in [9]. The performance evaluation and selection of suitable mother wavelets for DWT are made by subjecting the obtained DWT coefficients to (a) reconstruction, (b) denoising, and (c) compression, which are explained in the subsections. Relating the sample length of the signal n_s with that of the filter length of the wavelet n_w an appropriate number of levels n for the signal decomposition can be chosen using (2) [7, 22, 23].

$$n = \text{fix}\left(\log_2 \left(\frac{n_s}{n_w - 1} \right) \right). \tag{2}$$

Table 1
Mother wavelets considered in AEPD analysis.

Daubechies	Symlet	Coiflet	Bi-Orthogonal	
db1	sym1	coif1	bior1.1	bior3.3
db2	sym2	coif2	bior1.3	bior3.5
db3	sym3	coif3	bior1.5	bior3.7
db4	sym4	coif4	bior2.2	bior3.9
db5	sym5	coif5	bior2.4	bior4.4
db6	sym6		bior2.6	bior5.5
db7	sym7		bior2.8	bior6.8
db8	sym8		bior3.1	

3.2.1 Reconstruction

In the reconstruction, it is attempted to determine the ability of the mother wavelet to transform the signal from the time-domain to the wavelet-domain without losing information (by preserving its features). Each mother wavelet is chosen to decompose the AEPD signal into DWT coefficients. Then these DWT coefficients of the decomposed signal are subjected to the inverse discrete wavelet transform (IDWT) to get back the time-domain signal, called the

reconstructed signal [9]. The difference between the original signal S_O and the reconstructed signal S_R gives the error in representing the signal in the wavelet-domain. This numerical experiment is conducted with each mother wavelet (the 36 listed in **Table 1**). As described in Section 3.1, 5 AEPD test (sample) signals are utilized for DWT analysis in this study. The mother wavelet that results in the least error (between the original and reconstructed signal) is considered the best for the AEPD signal analysis. This process is depicted in Fig. 4 by a block diagram.

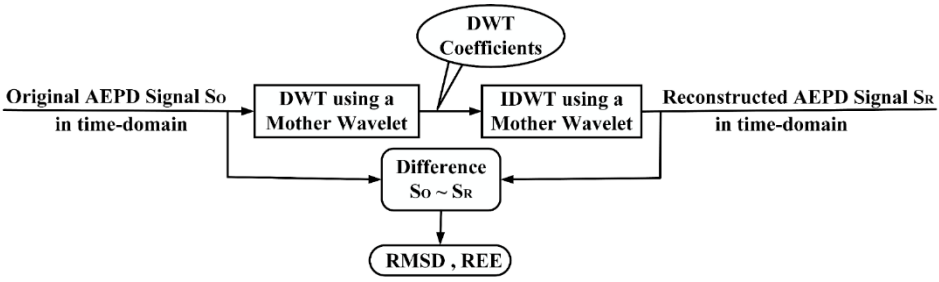

Fig. 4 – *Block diagram depicting error quantification process to assess the performance of a mother wavelet in representing the signal in the wavelet-domain.*

The ability of the mother wavelet to represent the signal accurately in the wavelet-domain is quantified using metrics (a) the root mean square difference (RMSD) and (b) relative error in energy (REE) as defined in (3) and (4), respectively [23].

$$RMSD = \sqrt{\frac{\sum_{n=1}^{N}\left(S_O(n) - S_R(n)\right)^2}{\sum_{n=1}^{N}(S_O(n) - \bar{S}_O)^2}}, \tag{3}$$

$$REE = \frac{\sum_{n=1}^{N} S_O^2(n) - \sum_{n=1}^{N} S_R^2(n)}{\sum_{n=1}^{N} S_O^2(n)}. \tag{4}$$

In (3), $\bar{S}_O$ denotes the mean value of the original signal S_O, and N denotes the number of sampling instants in the time-domain (N = 1024 in the present case). The outcome of this numerical experiment is given in the results under Subsection 4.1.

3.2.2 Denoising

The denoising aspect of DWT is essential when the signals are acquired in a harsh, noisy environment. Different types of interference and noise that can be encountered during a live PD measurement are (a) discrete spectral interferences (DSI), (b) periodic pulse-shaped interferences, (c) stochastic (random) noise, and (d) white noise [11, 12, 19, 26]. The PD signals in the acoustic form (AEPD) are less prone to noise than are the PD signals in their electric form [5]. However,

there can be some acoustic noise in AEPD signals and thus they need to be pre-processed in the wavelet-domain. After performing DWT and denoising, the signal may have varying degrees of noise traces specific to each mother wavelet. Hence the mother wavelet that performs best in coping with noisy signals needs to be evaluated.

The 5 AEPD test signals used in the analysis are collected in the laboratory environment with very little (or no) noise. Hence, in the present work, artificially simulated additive white gaussian noise (AWGN) is added to the noiseless test signal S_O generated in the experimental setup for the sake of comparing wavelet performance. To the AEPD test signal, the AWGN of 10 percentage energy is added, resulting in a noisy signal S_N having a signal-to-noise ratio (SNR) of 10dB [21]. This noisy AEPD signal S_N in time-domain is decomposed using a mother wavelet with a corresponding level of decomposition as given in (2). This results in noisy DWT coefficients. After the process of denoising, these denoised DWT coefficients are subjected to IDWT, and the resultant reconstructed signal S_D is compared with the original signal S_O [10]. The process adopted for the purpose of denoising-based analysis is described by a block diagram as shown in Fig. 5.

The denoising performance is evaluated by comparing the signals S_O and S_D using the metrics (a) signal-to-noise ratio (SNR) and (b) energy ratio (ER), as given by (5) and (6), respectively.

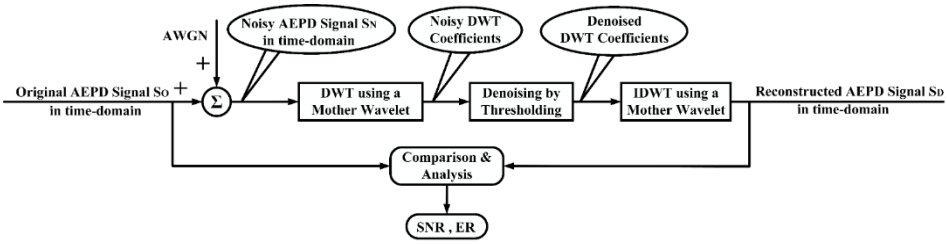

Fig. 5 – *Block diagram depicting performance assessment of a mother wavelet while AEPD signal denoising (in wavelet-domain).*

$$SNR = 10\log_{10}\left(\frac{\sum_{n=1}^{N} S_O^2(n)}{\sum_{n=1}^{N} S_O^2(n) - \sum_{n=1}^{N} S_D^2(n)}\right), \tag{5}$$

$$ER = \frac{\sum_{n=1}^{N} S_D^2(n)}{\sum_{n=1}^{N} S_O^2(n)}. \tag{6}$$

To demonstrate how the signal and noise manifest themselves differently in the wavelet-domain, the DWT is applied to the test-AEPD signal and noise separately using ‘sym8’ as the mother wavelet with a 6-level decomposition (as

given in (2) for a signal of n_s = 1024 samples and wavelet filter length of n_w = 16). This is only a typical example case. For each mother wavelet, the appropriate decomposition level n is identified based on its filter length n_w. The absolute values of their DWT coefficients obtained by MRA are plotted on the x-axis separately, as shown in Fig. 6. The vertical lines represent the partition of coefficients into sub-bands A6, D6, D5, D4, D3, D2, and D1, from left to right, as described in Section 2.2 of the wavelet transform. As seen from Fig. 6, the D2 and D3 sub-bands contain the most signal information, whereas the noise is almost uniformly spread across all the sub-bands. These attributes are used in implementing denoising in two different ways: (a) amplitude thresholding and (b) frequency thresholding, as described in Sections 3.2.2.1 and 3.2.2.2, respectively.

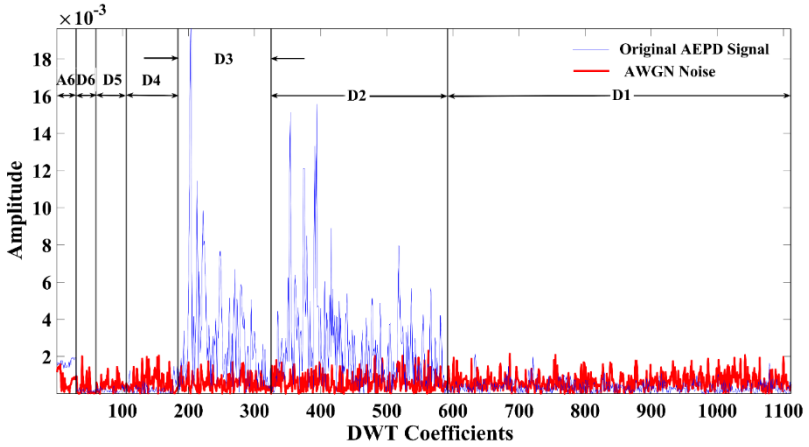

Fig. 6 – *DWT coefficients of a test AEPD signal and AWGN signal across frequency sub-bands (obtained using 'sym8').*

3.2.2.1 Amplitude thresholding

The detailed DWT coefficients obtained by MRA were subjected to amplitude soft-thresholding. The approximation sub-band coefficients are retained, as they contain the global information. Soft-thresholding is an exercise in which coefficients whose absolute values are lower than the threshold λ are first set to zero, and then one further shrinks the non-zero coefficients towards zero [7, 10]. As the DWT decomposition by MRA results in various levels (sub-bands), level-dependent soft-thresholding is adopted [12]. The threshold value is calculated using the empirical (7) for each level individually [21, 22].

$$\lambda_j = \alpha\sigma_j\sqrt{2\log_2(N_j)}\,. \tag{7}$$

Here N_j denotes the length of the coefficients in the j^{th} level and σ_j (which is equal to d_j /0.6745) denotes the standard deviation of the noise at that level, where

d_j is the median absolute deviation (MAD) of the coefficients present in the particular j^{th} level [22]. The term α depends on the extent of denoising required and is set to 0.05 by the trial-and-error method. The resulting denoised DWT coefficients are used to reconstruct the time-domain signal S_D by IDWT [15, 22]. The reconstructed signal S_D is compared with S_O using the performance indicators SNR and ER as given in (5) and (6) respectively.

3.2.2.2 Frequency thresholding

It is observed from Fig. 6 that most of the AEPD signal's information is in the D2 and D3 sub-bands, and the noise signal is widely spread among all the sub-bands. A proposed denoising approach eliminates the DWT coefficients other than D2 and D3 sub-bands. Approximation sub-band coefficients are retained as they contain the global information. The IDWT is applied to the retained DWT coefficients to reconstruct the denoised signal S_D in the time-domain. The reconstructed signal S_D is compared with S_O using the performance indicators SNR and ER as given in (5) and (6) respectively.

The outcome of the numerical experiments related to denoising is given in the results under Subsection 4.2.

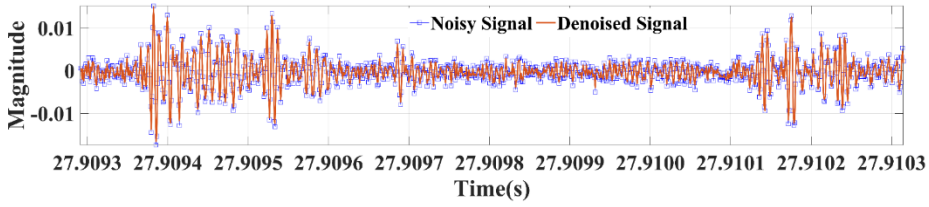

(a)

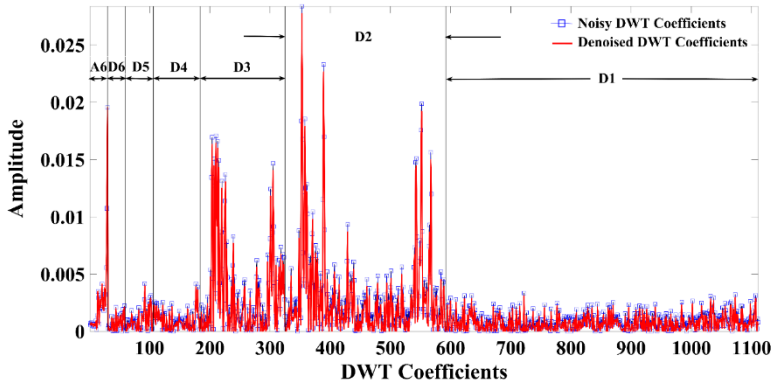

(b)

Fig. 7 – (a) *Signal in time domain before and after denoising using amplitude thresholding;* (b) *Signal in frequency domain before and after denoising using amplitude thresholding;*

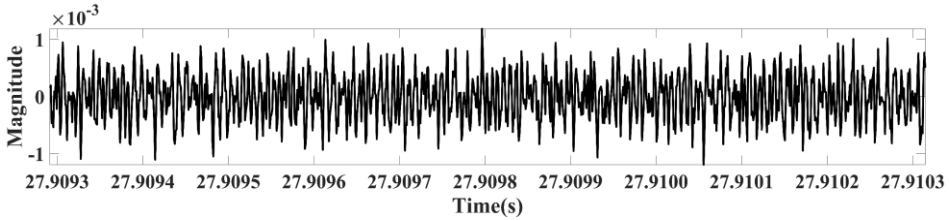

(c)

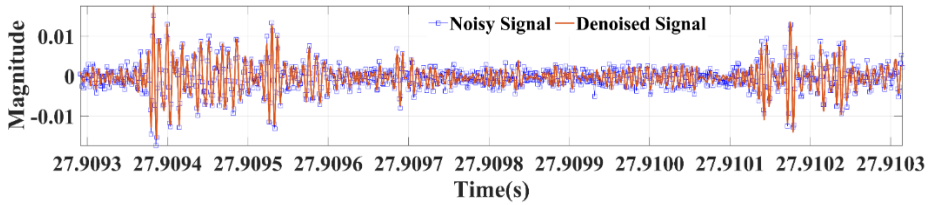

(d)

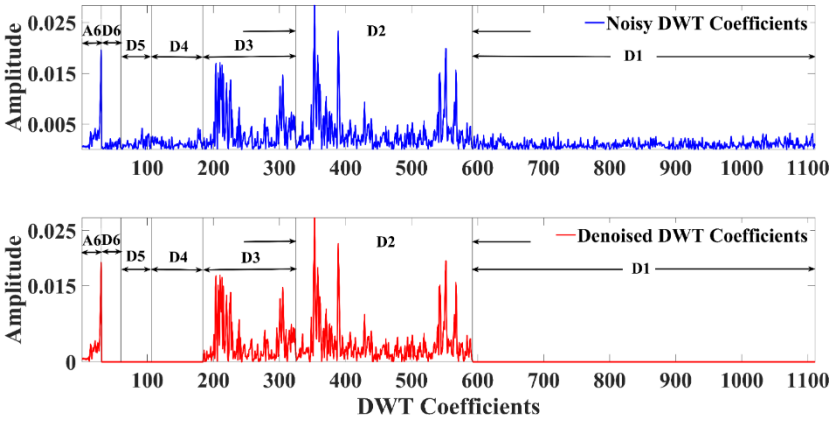

(e)

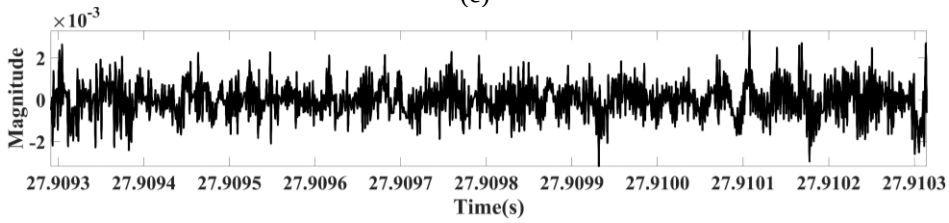

(f)

Fig. 7 – (c) *Residue between the noisy and denoised signals in the time domain using amplitude thresholding;* (d) *Signal in time domain before and after denoising using frequency thresholding;* (e) *Signal in frequency domain before and after denoising using frequency thresholding;* (f) *Residue between the noisy and denoised signals in the time domain using frequency thresholding.*

Fig. 7 illustrates the AEPD signal's representation before and after undergoing denoising via amplitude thresholding, portrayed in both the time domain (Fig. 7a) and frequency domain (Fig. 7b). The residue between the noisy and denoised signals in the time domain is presented in Fig. 7c. Furthermore, the application of frequency thresholding for denoising is depicted in both the time domain (Fig. 7d) and frequency domain (Fig. 7e), along with the residue between the noisy and denoised signals in the time domain (Fig. 7f). The 'db8' mother wavelet with a 6-level decomposition is used for this example.

3.2.3 Compression

Compression is a process of storing the information of a signal in a reduced data volume. Compression is significant when the data size is too large. The DWT helps in compressing the data set. The compressed DWT coefficients in the wavelet-domain should retain all the valuable information of the original signal. Each mother wavelet does this differently. The process adopted for the compression -based analysis is described by a block diagram, as shown in Fig. 8.

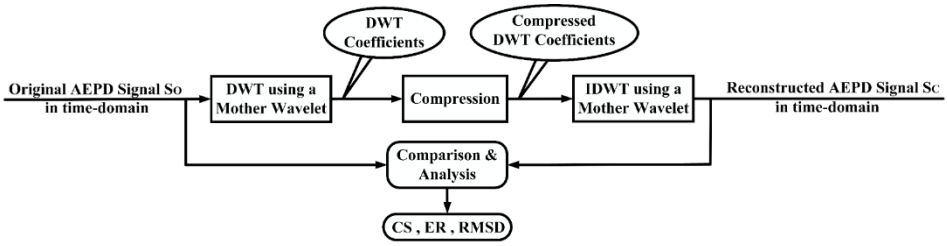

Fig. 8 – *Block diagram depicting performance assessment of a mother wavelet while AEPD signal is compressed (in wavelet-domain).*

DWT is applied to the original AEPD signal S_O, resulting in DWT coefficients. The detailed coefficients are subjected to universal hard-thresholding, where the coefficients are compared against a predetermined threshold value. Hard-thresholding is a process in which the coefficient values are set to zero if their absolute values are less than the threshold value, and the remaining coefficients are retained. The approximation coefficients are not disturbed as they contain the signal's global properties. After thus compressing the coefficient set in the wavelet-domain, the resulting DWT coefficients are subjected to IDWT to reconstruct the compressed signal S_C in the time-domain.

The compression performance is evaluated by comparing the signals S_O and S_C using the metrics (a) compression scores (CS), (b) ER, and (c) RMSD given by (8) – (10), respectively [23].

$$CS = \frac{100\left(\text{Number of coefficients set to zero by thresholding}\right)}{\text{Total number of coefficients}}, \qquad (8)$$

$$ER = \frac{\sum_{n=1}^{N} s_C^2(n)}{\sum_{n=1}^{N} s_O^2(n)}\ , \tag{9}$$

$$RMSD = \sqrt{\frac{\sum_{n=1}^{N}\left(s_O(n) - s_C(n)\right)^2}{\sum_{n=1}^{N}\left(s_O(n) - \overline{S_O}\right)^2}}\ . \tag{10}$$

In (10), $\overline{S_O}$ denotes the mean value of the original AEPD signal S_O. The outcome of the numerical experiments related to compression is given in the results section under Subsection 4.3.

3.2.4 Energy based final selection

The mother wavelet that results in the highest concentration of energy within sub-bands can be selected as the most suitable mother wavelet [23]. This concept is used as the overriding criterion to finalize the choice from among the wavelets chosen from (i) reconstruction, (ii) denoising, and (iii) compression described in Sections 3.2.1 to 3.2.3.

The sampling frequency in the present study is 1 MHz. Therefore, the maximum detectable frequency is 500 kHz. The Fourier spectrum of the signal reveals that most of the energy is present in the frequency range of 62.5 kHz to 250 kHz. It is noticed that for all 5 samples (Section 3.1), the frequency range is the same. The specific frequency ranges of the sub-bands of DWT (Section 2.2) applicable to the present study are shown in **Table 2**. It is observed from **Table 2** that the frequency range 62.5-250 kHz corresponds to D2 and D3 sub-bands. This implies that most of the energy is concentrated in these sub-bands. A similar inference can be drawn from Fig. 6. Hence the mother wavelet that results in the highest concentration of energy within sub-bands D2 and D3 can be selected as the most suitable mother wavelet for all three performances individually [23]. The outcome of the numerical experiments related to the energy-based final selection is given in the results section in Subsection 4.4.

Table 2
Sub-bands and associated frequencies.

Decomposed components	Frequency range [kHz] (Sampling frequency: 1 MHz)
D1	250 – 500
D2	**125 – 250**
D3	**62.5 – 125**
D4	31.2 – 62.5
D5	15.6 – 31.2
D6	7.81 – 15.6
A6	0 – 7.81

3.3 Flow chart of shortlisting and final selection of mother wavelet for AEPD signal analysis

This study evaluated 36 mother wavelets belonging to 4 different families. The best mother wavelet from each family was shortlisted for all three performances (reconstruction, denoising, and compression) based on appropriate metrics. Further, based on energy criteria, the best mother wavelets are obtained from among all the families for all three performances mentioned above. The flow chart describing the selection process of the most suitable mother wavelet for analysis of AEPD signals in the wavelet domain is given in Fig. 9.

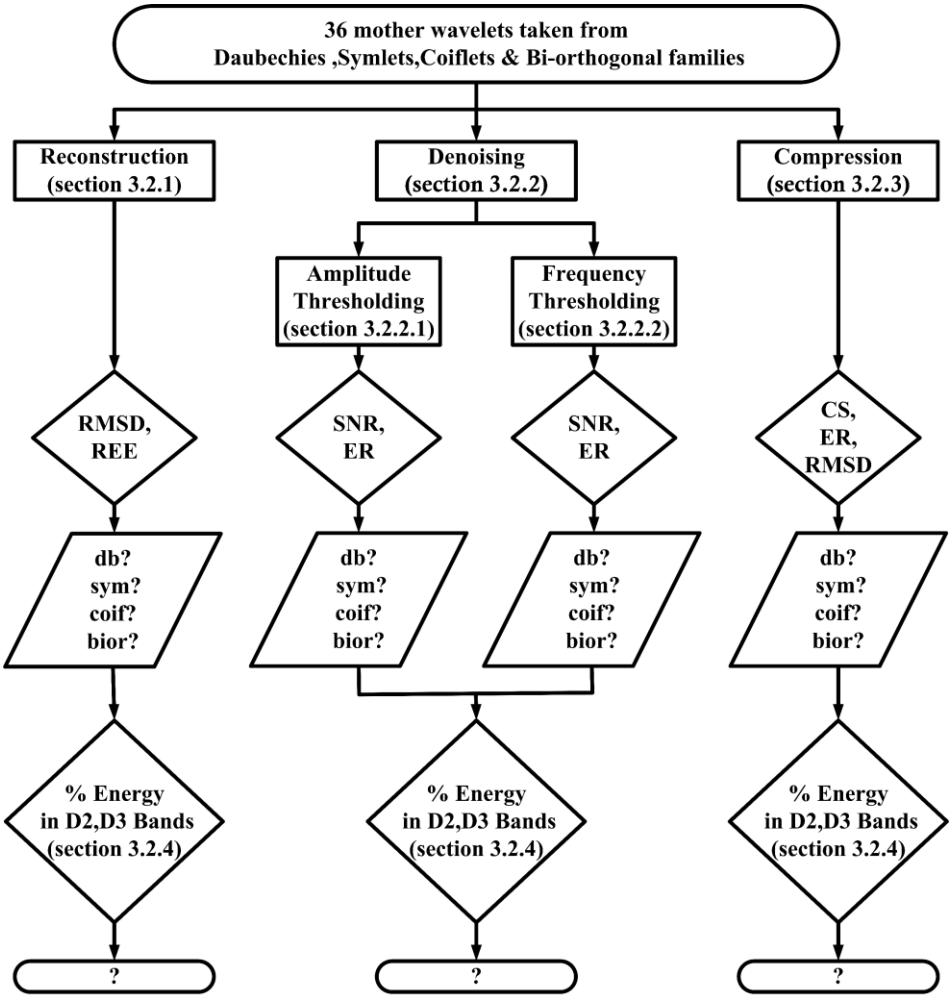

Fig. 9 – *Flow chart describing the selection process of mother wavelet in AEPD signal analysis.*

4 Results

The decomposition and reconstruction of AEPD signals for analysis are performed in MATLAB. The “eps” in MATLAB during these numerical experiments is 2.22e-16. In MATLAB, "eps" refers to the precision of floating numbers. The numerical experiments conducted to compare the metrics RMSD and REE indicate a 5-order difference. Such a considerable difference motivates choosing an appropriate mother wavelet for DWT analysis of AEPD signals.

4.1 Selection based on reconstruction

Assessing the ability of a mother wavelet to represent the signal accurately in the wavelet-domain was described in Section 3.2.1. This comparison is quantified using the metrics (a) root mean square difference (RMSD) and (b) the relative error in energy (REE) as defined in (3) and (4), respectively. The average values (RMSD and REE) of 5 test signals are used in the analysis. The best member of each wavelet family (listed in **Table 1**) which results in the least error are given in **Table 3**.

Table 3

Best performing mother wavelets of each family in terms of ‘reconstruction’.

Mother wavelet	% RMSD	% REE
db1	3.72e-14	4.89e-14
sym1	3.73e-14	4.89e-14
coif3	2.24e-10	1.19e-10
bior2.4	3.48e-14	3.94e-14

4.2 Selection based on denoising

The procedure of evaluating the denoising suitability of the mother wavelet was described in Section 3.2.2. This comparison is quantified using the metrics (a) signal-to-noise ratio (SNR) and (b) energy ratio (ER) given by (5) and (6), respectively. The average values (SNR and ER) of 5 test signals are used in the analysis. The mother wavelet with the highest SNR and % ER nearest to 100 is considered the best-performing.

4.2.1 Selection based on amplitude thresholding

In denoising using amplitude thresholding (described in Section 3.2.2.1), the best member of each wavelet family (listed in **Table 1**) is taken to be that which results in the highest SNR and a % ER near 100. They are given in **Table 4**. In general, denoising should result in the improvement of the SNR. It is noticed that SNR values have improved above 13dB for all the mother wavelets considered from the initial added value of 10dB (AWGN). From % ER values, it is observed that more than 94 % of the energy of the test signal is retained in the denoised signal for all the mother wavelets under study.

Table 4
Best performing mother wavelets of each family in terms of 'amplitude threshold based denoising'.

Mother wavelet	SNR [dB]	% ER
db8	14.8	95.3
sym6	16.0	94.8
coif4	14.9	95.3
bior1.5	15.0	95.6

4.2.2 Selection based on frequency thresholding

The denoising using frequency thresholding was described in Section 3.2.2.2. This proposed method eliminates the DWT coefficients in the sub-bands other than D2 and D3. This method may result in the reduction of signal content to some extent. Hence, SNR with few mother wavelets was observed to be reduced to around 8dB. On the contrary, in most cases, the SNR has increased above the initial added value of 10dB (AWGN). The best member of each wavelet family (listed in **Table 1**), namely, that which results in the highest SNR and a % ER near 100, is given in **Table 5**.

Table 5
Best performing mother wavelets of each family in terms of 'frequency threshold based denoising'.

Mother wavelet	SNR [dB]	% ER
db5	26.9	100.3
sym4	22.7	99.4
coif2	21.7	99.8
bior3.5	28.9	99.9

4.3 Selection based on compression

Assessing the compression ability of the mother wavelet in the wavelet-domain was described in Section 3.2.3. This comparison is quantified using the metrics (i) compression scores (CS), (ii) energy ratio (ER), and (iii) root mean square difference (RMSD) as defined in (8) – (10), respectively. The average values (CS, ER, and RMSD) of 5 test signals are used in the analysis. The best member of each wavelet family (listed in **Table 1**), namely, that which results in the highest % ER and least % RMSD, is given in **Table 6**. On average, 80% of the compression score is achieved with standard deviation less than 4, which is quite satisfactory. It is noticed that the best members for compression capability are the highest-order wavelets in their corresponding families. This is in line with the vanishing moments property of the mother wavelet. The vanishing moment

of a wavelet is the index number postfixed to the family name of the wavelet (for example, the vanishing moment of the 'sym6' wavelet is 6). The higher the vanishing moment, the higher the order of the polynomials that can be well approximated. This results in as many as zero detailed-coefficients and as few approximation-coefficients as possible. Eventually, this phenomenon results in higher compression scores.

Table 6
Best performing mother wavelets of each family in terms of 'compression'.

Mother wavelet	% ER	% RMSD
db8	97.0	17.2
sym8	96.9	17.4
coif5	97.1	16.9
bior6.8	96.4	18.3

4.4 Energy based final selection

The best members of each family for all three types of performances (reconstruction, denoising, and compression) are gathered and given in **Table 7**.

Table 7
Shortlisted mother wavelets for AEPD signal analysis based on the three types of performances.

	Family name of mother wavelet			
	Daubechies	**Symlets**	**Coiflets**	**Bi-orthogonal**
Reconstruction	db1	sym1	coif3	bior2.4
Denoising	db5	sym4	coif2	bior1.5
	db8	sym6	coif4	bior3.5
Compression	db8	sym8	coif5	bior6.8

The mother wavelet that results in the highest concentration of energy within the desired sub-bands should be selected as the most suitable mother wavelet [22]. This overriding criterion was described in Section 3.2.4. In order to apply this criterion, the energy present in the D2 and D3 sub-bands (as a percentage of the energy of their DWT coefficients) is computed for all 5 test signals, and their average values are compared. The mother wavelets 'coif3', 'coif4', and 'coif5' turns out to be the best mother wavelets across all the families collectively for reconstruction, denoising, and compression purposes, respectively. These are listed in **Table 8**, along with the energy content of their D2 and D3 sub-bands.

Table 8
Suitable mother wavelets based on D2 and D3 sub-band energy criterion.

	Mother wavelet with highest energy in the D2, D3 sub-bands	**% Energy**
Reconstruction	coif3	96.5
Denoising	coif4	96.7
Compression	coif5	97.2

5 Conclusion

Selection of the most suitable mother wavelet for DWT analysis of AEPD signals is performed quantitatively using the "accuracy of wavelet decomposition results". The performance of 36 mother wavelets of 4 different families is compared by conducting numerical experiments using AEPD test signals collected in the laboratory.

– A set of best-performing mother wavelets are identified from the four families (Daubechies, Symlets, Coiflets, Bi-orthogonal), and three types of performances (reconstruction, denoising, and compression).

– Further, based on the % energy criteria, 'coif3', 'coif4', and 'coif5' are identified as the best-performing mother wavelets for reconstruction, denoising, and compression, respectively.

– Specific to the AEPD signal analysis, the representation in the DWT-domain is of utmost importance. Hence, the coif3 mother wavelet, whose performance is better in signal reconstruction, is better suited for AEPD signal analysis.

– The mother wavelet selection based on "accuracy of wavelet decomposition results" is presented in this work probably for the first time.

6 Acknowledgements

The first author thanks the Ministry of Education, Government of India for providing scholarship through NITK for the doctoral research.

7 References

[1] Y. Han, Y. H. Song: Condition Monitoring Techniques for Electrical Equipment - A Literature Survey, IEEE Transactions on Power Delivery, Vol. 18, No. 1, January 2003, pp. 4 – 13.

[2] L. Yang, M. D. Judd: Recognising Multiple Partial Discharge Sources in Power Transformers by Wavelet Analysis of UHF Signals, IEE Proceedings – Science, Measurement and Technology, Vol. 150, No. 3, May 2003, pp. 119 – 127.

[3] IEEE Recommended Practice for the Design of Reliable Industrial and Commercial Power Systems – Redline, IEEE Standard 493, 2007.

[4] T. Mutakamihigashi, S. Tajiri, S. Okada, H. Ueno: Relationship between AE Waveform Frequency and the Charges Caused by Partial Discharge in Mineral Oil, IEEE Transactions on Dielectrics and Electrical Insulation, Vol. 28, No. 5, October 2021, pp. 1844 – 1847.

[5] H. D. Ilkhechi, M. H. Samimi: Applications of the Acoustic Method in Partial Discharge Measurement: A Review, IEEE Transactions on Dielectrics and Electrical Insulation, Vol. 28, No. 1, February 2021, pp. 42 – 51.

[6] T. Boczar, D. Zmarzly: Application of Wavelet Analysis to Acoustic Emission Pulses Generated by Partial Discharges, IEEE Transactions on Dielectrics and Electrical Insulation, Vol. 11, No. 3, June 2004, pp. 433 – 449.

[7] G. Wang, S.- J. Kim, G.- S. Kil, S.- W. Kim: Optimization of Wavelet and Thresholding for Partial Discharge Detection under HVDC, IEEE Transactions on Dielectrics and Electrical Insulation, Vol. 24, No. 1, February 2017, pp. 200 – 208.

[8] M. Harbaji, K. Shaban, A. El-Hag: Classification of Common Partial Discharge Types in Oil-Paper Insulation System Using Acoustic Signals, IEEE Transactions on Dielectrics and Electrical Insulation, Vol. 22, No. 3, June 2015, pp. 1674 – 1683.

[9] M. Misiti, Y. Misiti, G. Oppenheim, J.- M. Poggi: Wavelet Toolbox – For Use with MATLAB, User's Guide, The MathWorks Inc., 2015.

[10] I. Shim, J. J. Soraghan, W. H. Siew: Detection of PD Utilizing Digital Signal Processing Methods. Part 3: Open-Loop Noise Reduction, IEEE Electrical Insulation Magazine, Vol. 17, No. 1, January-February 2001, pp. 6 – 13.

[11] L. Satish, B. Nazneen: Wavelet-Based Denoising of Partial Discharge Signals Buried in Excessive Noise and Interference, IEEE Transactions on Dielectrics and Electrical Insulation, Vol. 10, No. 2, April 2003, pp. 354 – 367.

[12] J. Seo, H. Ma, T. Saha: Probabilistic Wavelet Transform for Partial Discharge Measurement of Transformer, IEEE Transactions on Dielectrics and Electrical Insulation, Vol. 22, No. 2, April 2015, pp. 1105 – 1117.

[13] G. F. C. Veloso, L. E. Borges da Silva, I. Noronha, G. Lambert Torres: Using Partial Discharge as Sample Signal Source to Identify Contamination Moisture Pattern in Power Transformer Insulating Oil, Proceedings of the 36th Annual Conference on IEEE Industrial Electronics Society (IECON), Glendale, USA, November 2010, pp. 1041 – 1044.

[14] A. H. Mohd Hashim, N. Azis, J. Jasni, M. A. Mohd Radzi, M. Kozako, M. K. Mohd Jamil, Z. Yaakub: Partial Discharge Localization in Oil Through Acoustic Emission Technique Utilizing Fuzzy Logic, IEEE Transactions on Dielectrics and Electrical Insulation, Vol. 29, No. 2, April 2022, pp. 623 – 630.

[15] R. M. Sharkawy, T. K. Abdel-Galil, R. S. Mangoubi, M. M. Salama, R. Bartnikas: Particle Identification in Terms of Acoustic Partial Discharge Measurements in Transformer Oils, IEEE Transactions on Dielectrics and Electrical Insulation, Vol. 15, No. 6, December 2008, pp. 1649 – 1656.

[16] W. Keng Ngui, M. S. Leong, L. M. Hee, A. M. Abdelrhman: Wavelet Analysis: Mother Wavelet Selection Methods, Applied Mechanics and Materials, Vol. 393, September 2013, pp. 953 – 958.

[17] R. Liao, C. Guo, K. Wang, Z. Zuo, A. Zhuang: Adaptive Optimal Kernel Time–Frequency Representation Technique for Partial Discharge Ultra-High-Frequency Signals Classification, Electric Power Components and Systems, Vol. 43, No. 4, February 2015, pp. 449 – 460.

[18] A. Hussain, Z. Ahmed, M. Shafiq, A. Zaher, Z. Rashid, M. Lehtonen: An Adaptive Denoising Algorithm for Online Condition Monitoring of High-Voltage Power Equipment, Electric Power Components and Systems, Vol. 48, No. 9-10, October 2020, pp. 1036 – 1048.

[19] M. Hashmi, M. Lehtonen, M. Nordman, R. A. Jabbar, S. A. Qureshi: Wavelet-Based De-Noising of On-Line PD Signals Captured by Pearson Coil in Covered-Conductor Overhead Distribution Networks, International Journal of Electrical Power & Energy Systems, Vol. 43, No. 1, December 2012, pp. 1185 – 1192.

[20] I. Daubechies: Ten Lectures on Wavelets, 1st Edition, SIAM-Society for Industrial and Applied Mathematics, Philadelphia, 1992.

[21] J.- C. Hsieh, C.- C. Tai, M.- S. Su, Y.- H. Lin: Identification of Partial Discharge Location Using Probabilistic Neural Networks and the Fuzzy C-Means Clustering Approach, Electric Power Components and Systems, Vol. 42, No. 1, 2014, pp. 60 – 69.

[22] M.- S. Su, J.- F. Chen, Y.- H. Lin: Phase Determination of Partial Discharge Source in Three-Phase Transmission Lines Using Discrete Wavelet Transform and Probabilistic Neural Networks, International Journal of Electrical Power & Energy Systems, Vol. 51, October 2013, pp. 27 – 34.

[23] X. Zhou, C. Zhou, I. J. Kemp: An Improved Methodology for Application of Wavelet Transform to Partial Discharge Measurement Denoising, IEEE Transactions on Dielectrics and Electrical Insulation, Vol. 12, No. 3, June 2005, pp. 586 – 594.

[24] T. B. Shanker: Acoustic Emission Signal Based Investigations Involving Laboratory and Field Studies Related to Partial Discharges & Hot-Spots in Power Transformers, PhD Dissertation, National Institute of Technology Karnataka, Mangalore, India, 2016.

[25] T. B. Shanker, H. N. Nagamani, D. Antony, G. S. Punekar: Effects of Transformer-Oil Temperature on Amplitude and Peak Frequency of Partial Discharge Acoustic Signals, IEEE Transactions on Power Delivery, Vol. 33, No. 6, December 2018, pp. 3227 – 3229.

[26] R. V. Maheswari, P. Subburaj, B. Vigneshwaran, I. M. S. Willjuice: Support Vector Machine-Based Denoising Technique for Removal of White Noise in Partial Discharge Signal, Electric Power Components and Systems, Vol. 42, No. 14, September 2014, pp. 1611 – 1622.